Research on a ø6m TBM Steel Arch Splicing Manipulator

Yuanfu He
Central South University
Yimin Xia (2821858566@qq.com)
College of Mechanical and Electrical Engineering, Central South University, Changsha 410083, China
Zhen Xu
China Railway Construction Heavy Industry Co. Ltd.
Jie Yao
China Railway Siyuan Survey and Design Group Co. Ltd.
Bo Ning
Central South University
Xuemeng Xiao
Central South University

Original Article

Keywords: Steel arch splicing manipulator, Single-DOF closed-loop mechanism, Screw Theory, Graphical type synthesis method, Mechanism design

Posted Date: January 28th, 2021

DOI: https://doi.org/10.21203/rs.3.rs-155418/v1

Research on a ϕ6m TBM steel arch splicing manipulator

Yuanfu He[1,2], Yimin Xia[1,2,*], Zhen Xu[3], Jie Yao[4,5] , Bo Ning[1,2], Xuemeng Xiao[1,2]

[1] College of Mechanical and Electrical Engineering, Central South University, Changsha 410083, China

[2] State Key Laboratory of High Performance Complex Manufacturing, Central South University, Changsha 410083, China

[3] China Railway Construction Heavy Industry Co. Ltd., Changsha 410100, China

[4] China Railway Siyuan Survey and Design Group Co. Ltd., Wuhan 430063, China

[5] National-Local Jonit Engineering Research Center of Underwater Tunnelling Technology, Wuhan 430063, China

Abstract

As a challenging task, the robotic splicing of steel arch is required to realize the grasping and docking of steel arches in a limited space. The steel arches often have a mass of over 200kg and a length of over 4m. Due to the large volume and mass of steel arches and the high requirements for the positioning accuracy of splicing, it is difficult for the general manipulator to meet its flexibility and stiffness requirements. The single-degree-of-freedom(DOF) closed-loop mechanism has a simple and reliable structure. Adding it into the manipulator can effectively improve the dynamic performance and increase the structural stiffness. In this paper, a solution model of a single-DOF closed-loop planar mechanism is presented, and alternative kinematic pairs of the mechanism with different input constraints and output requirements are derived. Based on this model, a design method of steel arch splicing manipulator with single-DOF closed-loop grasping structure is proposed. All the optional basic configurations of the manipulator are deduced, and then the optimal configuration is obtained by using the performance indexes. A prototype of the steel arch splicing manipulator is manufactured, and the reliability of the manipulator is proved by experiments.

Keywords Steel arch splicing manipulator · Single-DOF closed-loop mechanism · Screw Theory · Graphical type synthesis method · Mechanism design

Declarations

Funding: the National Key Research and Development Program of China (Grant No. 2017YFB1302600), the Major Science and Technology Projects of Hunan Province (Grant No. 2019GK1010).

Conflicts of interest/Competing interests: We declare that we have no fnancial and personal relationships with

* Corresponding author: Yimin Xia
E-mail address: xiaymj@csu.edu.cn.

other people or organizations that can inappropriately infuence our work, and there is no professional or other personal interest of any nature or kind in any product, service and/or company that could be construed as infuencing the position presented in, or the review of, the manuscript entitled “Research on a ϕ6m TBM steel arch splicing manipulator.”

Availability of data and material: Not applicable.

Code availability: Not applicable.

1 Introduction

Generally known as a large-scale equipment, Hard Rock Tunnel Boring Machine (TBM) is specially applied to conduct the tunnel excavation inside hard rock[1-4].With the functions of excavating, slagging and supporting, TBM is also widely adopted in the field of hard rock excavation[5-7]. The construction of TBM would unavoidably destroy the initial in-situ stress state of the surrounding rock in the original stratum, resulting in redistribution of stress in the surrounding rock which would lead to the deformation, destruction or even collapse of the surrounding rock[8,9]. Especially with the unsatisfying quality of surrounding rock and the severe fragmentation of rock mass, the self-stabilization period of surrounding rock is quite short or fails to appear. Therefore, it is necessary to provide timely and effective steel arch support to control the deformation of the surrounding rock and prevent the damage of the surrounding rock[10,11]. At present, the splicing of TBM steel arches is carried out manually, as shown in Fig. 1. Inside a narrow operation area of the construction personnel, the working environment is extremely harsh with strong vibration, numerous dust, low brightness as well as high humidity, where the labors are often required to stand in the stagnant water. Each steel arch is endowed with a mass of up to 200kg, requiring the manual movement, adjustment, and docking. The extremely high difficulty of the process would lower the splicing efficiency of the steel arch frame low, additionally, it would also lead to the delayed support delay or the unstable quality and finally cause collapse accident.

(a) Steel arch construction environment (b) Docking process of steel arch

Fig.1 Manual splicing of steel arch

At present, steel arch installation is mainly carried out by means of manual coordination with ring beam erector. The steel arches are delivered to ring beam erector by transport truck and TBM crane, and the workers transport the steel arches to the assembly ring of ring beam erector and fixes it. Then the assembly ring rotates at a certain angle to place the second steel arch. Workers adjust the attitude of the adjacent steel arches on the assembly ring so that the two steel arches are close to each other and the bolt holes are aligned, and then they are bolted together. As the steel arch is very heavy, it is difficult to grasp and drag, so many people are often required to carry and adjust the steel arch, and even use jacks to assist in joining the steel arch, which seriously affects the construction efficiency. In order to relieve the workload and improve the constructional quality, efficiency and safety, the concept of automatic installation of TBM steel arches is firstly proposed. A steel arch splicing manipulator is designed to realize the automatic splicing of steel arches, and improve the intelligence and assembly efficiency of TBM construction.

As the first case which investigates on the TBM steel arch splicing manipulator, related achievements have still not been publicly reported, while a series of researches could be found associated with the design of the grasping manipulator[12]. Huang[13] has proposed a general design method for spatial 3-DOF isotropic manipulators, and developed 6-DOF or redundant manipulators applying 3-DOF robots as modules. Considering the operation and grasping requirements of the mechanism, Ozgür [14], Lambert[15] have analyzed the DOF and structure of the planar as well as the space manipulator, and designed a manipulator that could meet the grasping performance. Gao[16], Liang[17] considered the shape diversity of the grasped object, and designed a manipulator to realize the self-adaptive enveloping grasp. Kaluarachchi[18] has presented a design method of lightweight tendon-driving redundant manipulator. With the reduced joint torque applying a single motor, the number of actuators could get reduced and power consumption would also be minimized. Babin[19] has proposed a design method for the manipulators which could grasp small objects within the confined spaces, applying a planetary gear train to replace the traditional revolute joints. However, apart from the large mass, the steel arch is with the structure of a slender I-beam. Therefore, with the inability to guarantee the grasping stability and the docking accuracy of the steel arch, these design schemes are unsuitable for splicing steel arches.

The grasping action of steel arch needs two jaws to cooperate with each other. In order to improve the dynamic performance, increase the structural stiffness and reduce the input control, a single-DOF closed-loop planar mechanism is considered to be introduced into the grasping structure of the manipulator. At present, researches on single-DOF closed-loop mechanism are mainly focused on leg mechanism and gripper mechanism[20]. Studies of closed-loop planar mechanisms such as Chebyshev Mechanism[21], Klann

Mechanism[22], LARM BiPED Mechanism[23] and DQV[24] have shown that the closed-loop series structure possesses the integral rigidity, more suitable for missions under a high load, and it performs better at high stride frequency[25,26].Liu[27] designed a single DOF robot leg mechanism intended for tailed quadruped locomotion. The design employs a four-bar planar mechanism that couples the hip and knee flexion/extension joints mechanically, which reduce the leg's DOF without violating the foot trajectory. The actuator is concentrated at a proximal location, increasing the rigidity-to-weight ratio. Hassan[28,29] introduced the crank slider mechanism into the gripper, realizing the purpose of a single driver controlling the tensioning of four fingers simultaneously. Anwar[30] proposed a soft closed-chain modular gripper, and designed a single-DOF closed-loop plane structure on each finger, so that it can passively adapt around a curved surface, with the benefits of flexibility, low weight and controllability. However, most of the above work dedicated to reconfiguration analysis of individual mechanism and to designs combining existing mechanisms[31]. The fundamental for structure synthesis of a single-DOF closed-loop mechanism has not been systematically explored. Nor has a mathematical model been derived that could serve as a basic modular foundation block for exploring similar closed-chain manipulators and grippers.

Among the innovative design theories and methods of articulated rigid body systems, screw theory [32-35] and graphical type synthesis method[36,37] present irreplaceable advantages in the design of complex manipulator due to the simple and intuitive characteristics, while they are basically only used in the design of parallel manipulators at present. The grasping action of the steel arch splicing manipulator requires the mutual cooperation between both the upper and lower jaws and also the functions of adjusting and docking the steel arch. Regarding to this complex manipulator with multiple interrelated output tips, screw theory and graphical type synthesis method can realize the analysis and synthesis of the manipulator from the basic principle. At present, seldom research could be figured in this field.

In this paper, a solution model of single-DOF closed-loop planar mechanism is presented, which is used to analyze the law of kinematic pairs' number, arrangement and axis layout of the mechanism. Based on this model, the design scheme of single-DOF closed-loop grasping mechanism and posture adjusting mechanism for steel arch is proposed. A steel arch splicing manipulator which can realize the automatic installation of steel arch is developed, and the reliability of the manipulator is verified by experiments.

2 Solution model of single-DOF closed-loop mechanism

2.1 Analysis of single-DOF closed-loop mechanism

Mobility of a mechanism is generally calculated in terms of the Chebychev–Grübler–Kutzbach criterion[38]

expressed in the formula

$$F = d(n - g - 1) + \sum_{i=1}^{g} f_i \tag{1}$$

where F is the mobility of a mechanism, d is the DOF of the space in which the mechanism works, n is the number of bodies connected by g joints and f_i is the connectivity or DOF of the ith joint.

The single-DOF closed-loop mechanism is composed of rotating pairs and moving pairs with one DOF $(f_i=1)$. The number of bars n and the number of kinematic pairs g must be equal, meaning

$$g=d+1 \tag{2}$$

The screw theory is used to analyze the single-DOF closed-loop mechanism. Screw $\$_{Ri}$ of the ith revolute pair and screw $\$_{Pj}$ of the jth prismatic pair on the mechanism are respectively expressed as

$$\$_{Ri}=\left(\boldsymbol{s}_{Ri};\quad \boldsymbol{s}_{0Ri}\right) \tag{3}$$

$$\$_{Pj}=\left(\mathbf{0};\quad \boldsymbol{s}_{Pj}\right) \tag{4}$$

The sum of the spatial DOF d and the over-constrained number λ of the single-DOF closed-loop mechanism is 6. If the virtual work done by the over-constraint screws in the single closed-loop mechanism on the motion-screw system is 0, then such over-constraint will not affect the motion of the mechanism, thus ensuring the correctness of the mechanism.

If the motion-screw system of the mechanism is set as $\boldsymbol{S}=\{\$_1;\$_2;\mathrm{L}\ ;\$_g\}$, and the constraint-screw system is set as $\boldsymbol{S}_r=\{\$_{r1};\$_{r2};\mathrm{L}\ ;\$_{r\lambda}\}$, then for $\forall k\in\{1,2,\mathrm{L}\ ,\lambda\}$ and $\forall j\in\{1,2,\mathrm{L}\ ,g\}$, the virtual work done by the kth constraint screw of the single closed-loop mechanism on the jth motion screw is derived as

$$\delta W=\$_j \circ \$_{rk}=0 \tag{5}$$

The over-constraints are divided into independent force constraints and independent couple constraints, and the kinematic pairs are divided into revolute pairs and prismatic pairs. According to Eq.(5), it can be obtained that the virtual work should meet the following two conditions.

$$\begin{cases} \boldsymbol{s}\circ\boldsymbol{s}_r=\cos\alpha=0 \\ \boldsymbol{s}\circ\boldsymbol{s}_{0r}+\boldsymbol{s}_r\circ\boldsymbol{s}_0=-a\sin\alpha=0 \end{cases} \tag{6}$$

where α and a are respectively the spatial angle and distance between the motion screw and the constraint screw.

All screws on the closed-loop mechanism must be linearly related, so that

$$\sum_{j=1}^{g}\omega_j\$_j=0 \tag{7}$$

where $\omega_j\,(j=1,2,\mathrm{L}\ ,g)$ is the motion velocity of the jth joint of the closed-loop mechanism, and they are not all

zero. $\$_j$ is the motion screw of the *j*th joint.

By substituting Eq.(3) and Eq.(4) into Eq. (7), we obtain

$$\sum_{i=1}^{l} \omega_{Ri} \boldsymbol{s}_{Ri} = 0 \tag{8}$$

$$\sum_{i=1}^{l} \omega_{Ri} \boldsymbol{s}_{0Ri} + \sum_{j=1}^{g-l} \omega_{Pj} \boldsymbol{s}_{Pj} = 0 \tag{9}$$

2.2 Planar single-degree-of-freedom closed-loop mechanism

On engineering, single-DOF closed-loop planar mechanism is the most common. Due to its simple and reliable structure, it is often added into the open-chain mechanism to improve the dynamic performance and increase the structural stiffness. Given the input constraints and output requirements, how to design a closed-loop mechanism to meet the functional requirements has always been an urgent problem in engineering.

In a single-DOF closed-loop planar mechanism, the number of overconstraints $\lambda \in \{3,4\}$. When λ=3, the constraint-screw system contains 1 independent force constraint and 2 independent couple constraints, which are described as follows

$$\begin{cases} \$_{r1} = (\boldsymbol{s}_{r1}; \boldsymbol{s}_{0r1}) \\ \$_{r2} = (0; \boldsymbol{s}_{r2}) \\ \$_{r3} = (0; \boldsymbol{s}_{r3}) \end{cases} \tag{10}$$

For revolute pairs, the condition that the virtual work is 0 can be described as

$$\begin{cases} \delta \boldsymbol{W}_1 = -a_1 \sin \alpha_1 = 0 \\ \delta \boldsymbol{W}_2 = \cos \alpha_2 = 0 \\ \delta \boldsymbol{W}_3 = \cos \alpha_3 = 0 \end{cases} \tag{11}$$

All revolute pairs must be perpendicular to the two independent couple constraint screws, and intersecting or parallel to the force constraint screws.

For prismatic pairs, the condition that the virtual work is 0 can be described as

$$\begin{cases} \delta \boldsymbol{W}_1 = \cos \alpha_1 = 0 \\ \delta \boldsymbol{W}_2 = \delta \boldsymbol{W}_3 \equiv 0 \end{cases} \tag{12}$$

The axes of all prismatic pairs are perpendicular to the force constraint screws, and independent of the couple constraint screws.

$$g = d + 1 = 7 - \lambda \tag{13}$$

The number of kinematic pairs in the mechanism is 4, which can be RRRR RRRP RRPP RPPP PPPP. Where P represents prismatic joint and R represents revolute joint, and the RRRP institution is shown in Fig.2.

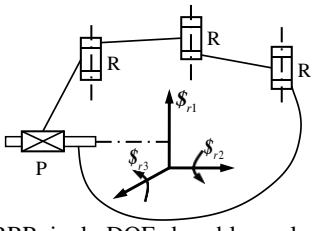

Fig.2 RRRP single-DOF closed-loop planar mechanism

When λ=4, g=7 − λ = 3. The constraint-screw system may contain either 1 independent force constraint and 3 independent couple constraints(denoted as F1), or 2 independent force constraints and 2 independent couple constraints(denoted as F2).

Similarly, in F1, the revolute pairs cannot be perpendicular to the 3 independent couple constraint screws, so there will be no revolute pair in the mechanism. The axis of prismatic pairs are required to be perpendicular to the force constraint, that is, the mechanism can only be PPP, as shown in Fig.3.

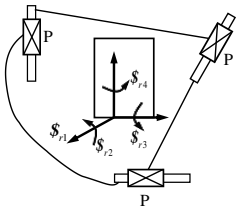

Fig.3 RRRP single-DOF closed-loop planar mechanism

In F2, the revolute pairs must be perpendicular to the 2 independent couple constraint screws, and intersecting or parallel to the 2 force constraint screws. The closed-loop mechanism under this condition is triangular stable structure, which does not meet the requirements.

2.3 The solution model of planar single-degree-of-freedom closed-loop mechanism

The joint part of the single-DOF closed loop planar mechanism is divided into input joint, output joint and intermediate joint part. Input screw $\$_i$=$\begin{pmatrix}0 & 0 & a_1; & b_1 & c_1 & 0\end{pmatrix}$, output screw $\$_o$=$\begin{pmatrix}0 & 0 & a_2; & b_2 & c_2 & 0\end{pmatrix}$, Where a_1 and a_2 can be 1 or 0. The intermediate joint part can be divided into revolute screw $\$_{Ri}$=$\begin{pmatrix}0 & 0 & 1; & y_{Ri} & -x_{Ri} & 0\end{pmatrix}$ and prismatic screw $\$_{Pi}$=$\begin{pmatrix}0 & 0 & 0; & x_{Pi} & y_{Pi} & 0\end{pmatrix}$, Where x_{Ri} and y_{Ri} represent the position of the revolute joint in the coordinate system, x_{Pi} and y_{Pi} represent the motion direction of the prismatic joint in the coordinate system, $y_{Pi}{}^2 + x_{Pi}{}^2 = 1$.

$$\omega_i\$_i + \sum_{i=1}^{l}\omega_{Ri}\$_{Ri} + \sum_{i=1}^{m}\omega_{Pi}\$_{Pi} = \omega_o\$_o \tag{14}$$

where l and m are respectively the number of revolute pairs and prismatic pairs in the intermediate part, $l+m\le 2$.

It can be deduced that

$$\sum_{i=1}^{l}\omega_{Ri}=a_2\omega_o-a_1\omega_i \tag{15}$$

$$\sum_{i=1}^{l}y_{Ri}\omega_{Ri}+\sum_{i=1}^{m}x_{Pi}\omega_{Pi}=b_2\omega_o-b_1\omega_i \tag{16}$$

$$-\sum_{i=1}^{l}x_{Ri}\omega_{Ri}+\sum_{i=1}^{m}y_{Pi}\omega_{Pi}=c_2\omega_o-c_1\omega_i \tag{17}$$

According to Eq.(15), the number of revolute joints in the intermediate part under different input and output joints can be obtained($\omega_{Ri}\neq 0$). When a_i=0 , the joint is a prismatic pair; when a_i=1 , the joint is a revolute pair.

Table 1 The number of revolute joints under different input and output joints

Input and output joint types	Condition	Number of rotating pairs
a_1=a_2=0	$\sum_{i=1}^{l}\omega_{Ri}=0$	$l\in\{0,2\}$
a_1=0， a_2=1 or a_1=1， a_2=0	$\sum_{i=1}^{l}\omega_{Ri}\neq 0$	$l\in\{1,2\}$
a_1=a_2=1	$\sum_{i=1}^{l}\omega_{Ri}=\omega_o-\omega_i$	$l\in\{0,1,2\}$

The velocity relationship of the intermediate joint can be obtained by combining Eq.(15)~(17).

$$\sum_{i=1}^{l}\left(\frac{a_2y_{Ri}-b_2}{a_1b_2-a_2b_1}+\frac{a_2x_{Ri}-c_2}{a_1c_2-a_2c_1}\right)\omega_{Ri}=\sum_{i=1}^{m}\left(\frac{a_2y_{Pi}}{a_1c_2-a_2c_1}-\frac{a_2x_{Pi}}{a_1b_2-a_2b_1}\right)\omega_{Pi} \tag{18}$$

When the input joint and output joint types are known, Eq.(18) is substituted into Eq.(16) and Eq.(17), and then the velocity relationship between input joint and output joint under different intermediate joint types can be obtained.

When $l=0$， $m=1$

$$\omega_o=\frac{b_1y_P-c_1x_P}{b_2y_P-c_2x_P}\omega_i \tag{19}$$

When $l=m=1$

$$\omega_o=\frac{-a_1\left(x_Px_R+y_Py_R\right)+b_1y_P-c_1x_P}{-a_2\left(x_Px_R+y_Py_R\right)+b_2y_P-c_2x_P}\omega_i \tag{20}$$

When $l=2$， $m=0$

$$\omega_o=\frac{a_1\left(x_{R2}y_{R1}-x_{R1}y_{R2}\right)+b_1\left(x_{R1}-x_{R2}\right)+c_1\left(y_{R1}-y_{R2}\right)}{a_2\left(x_{R2}y_{R1}-x_{R1}y_{R2}\right)+b_2\left(x_{R1}-x_{R2}\right)+c_2\left(y_{R1}-y_{R2}\right)}\omega_i \tag{21}$$

When $l=0$， $m=2$

$$\omega_o = \frac{\left(x_{P2}y_{P1} - x_{P1}y_{P2}\right)\left[a_1a_2\left(b_1b_2 + c_1c_2\right) - a_2a_2\left(b_1b_1 + c_1c_1\right)\right]}{\left(x_{P2}y_{P1} - x_{P1}y_{P2}\right)\left[a_1a_2\left(b_2b_2 + c_2c_2\right) - a_2a_2\left(b_1b_2 + c_1c_2\right)\right]}\omega_i \tag{22}$$

3 Design of steel arch splicing manipulator

A series of process are contained during the installation of TBM steel arch which are the transporting, grabbing, docking and bracing. The designed steel arch splicing manipulator is divided into the grasping module and the docking module, where it is required to flexibly grasp, adjust and connect two adjacent steel arches simultaneously. Moreover, in the process of steel arch transportation, the splicing manipulator would not interfere with the steel arch.

3.1 Design of the grasping module

According to the structure of the steel arch, it is envisaged to use two "L"-shaped jaws with a reverse arrangement to conduct the grasping of steel arch, as shown in Fig.4. Directly affected by the gravity of the steel arch, the lower jaw should be settled near the manipulator base to provide better carrying capacity while designing the gripping module. In order to furtherly obtain a superior grasping effect, the lower jaws would approach to the steel arch directly below the steel arch. In addition, force sensor devices are necessarily needed by the mechanism to real-timely monitor the grasping force and ensure the grasping performance of the steel arch splicing manipulator.

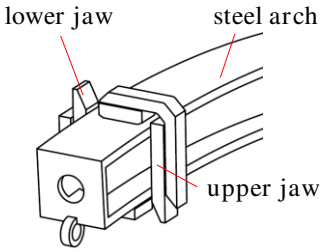

Fig.4 Schematic diagram of steel arch splicing

During the grasping process, the relative spatial positions of the upper and lower jaws need to be adjusted to avoid collisions with the steel arch. Owing to the synchronizing movement, both jaws would approach or move away from the steel arch at the same time. Envisaging the upper jaw to be driven by the movement of the lower jaw. Considering the reduction of input control, a single-DOF closed-loop grasping module design scheme is proposed. The linear motion of the lower jaw serves as the input and the motion of the upper jaw as the output. And in specific, the output motion form could be regarded with the form of rotation or movement.

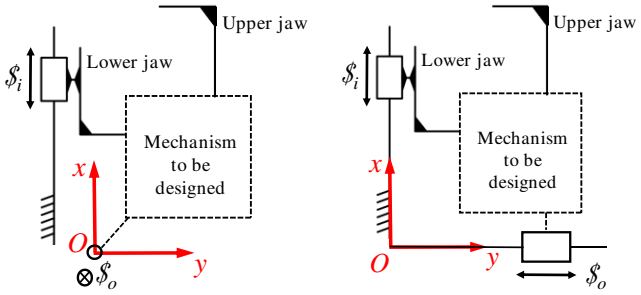

(a) Revolute output joint (b) Prismatic output joint

Fig.5 Schematic diagram of grasping module

A plane coordinate system is established for the single-DOF closed-loop structure of the steel arch splicing manipulator. The lower jaw is set to move along the x-axis. When the output joint that drives the upper jaw is a revolute joint, the center of the revolute joint would be taken as the origin. When the output joint is a prismatic joint, however, the origin would be determined as the intersection between the movement directions of the input prismatic joint and the output prismatic joint. As shown in Fig.5. $\$_i$ is the input motion screw which represents the screw of the lower jaw, $\$_i=(0\quad 0\quad 0;\quad 1\quad 0\quad 0)$. While $\$_o$ is the output motion screw which means the screw of the upper jaw.

When the output joint is a revolute pair, it could be obtained from Fig.5(a) that the output screw $\$_{o1}$ is

$$\$_{o1}=(0\quad 0\quad 1;\quad 0\quad 0\quad 0) \tag{23}$$

At this point, $a_1=0$，$a_2=1$. According to Table 1, the number of revolute joints in the middle part is 1 or 2. Combined with Eq.(20)~(21), the eligible single-DOF closed-loop structure is obtained, as shown in Table 2.

Table 2 Closed-loop structure of grasping module for revolute output joint

Number of intermediate kinematic pairs	Types of intermediate kinematic pairs	Relationship with ω_i and ω_o	Grasping module closed-loop structure
2	2R	$\omega_o=\dfrac{x_{R1}-x_{R2}}{x_{R2}y_{R1}-x_{R1}y_{R2}}\omega_i$	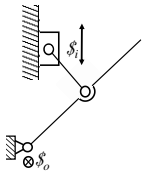
2	1R1P	$\omega_o=\dfrac{-y_P}{x_Px_R+y_Py_R}\omega_i$	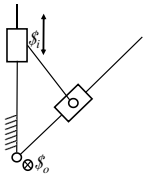

When the output joint is a prismatic joint, the output screw $\$_{o2}$ could be obtained from Fig.5(b) as

$$\$_{o2}=(0 \quad 0 \quad 0; \quad 0 \quad 1 \quad 0) \tag{24}$$

At this point, $a_1=a_2=0$. According to Table 1, the number of revolute joints in the middle part is 0 or 2. Combined with Eq.(19)~(22), the eligible single-DOF closed-loop structure is obtained, as shown in Table 3.

Table 3 Closed-loop structure of grasping module for prismatic output joint

Number of intermediate kinematic pairs	Types of intermediate kinematic pairs	Relationship with ω_i and ω_o	Grasping module closed-loop structure
1	1P	$\omega_o=-\frac{y_P}{x_P}\omega_i$	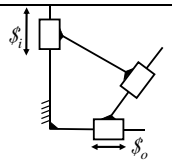
2	2R	$\omega_o=\frac{x_{R1}-x_{R2}}{y_{R1}-y_{R2}}\omega_i$	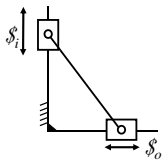
2	2P	$\omega_o=\frac{(x_{P2}y_{P1}-x_{P1}y_{P2})\times 0}{(x_{P2}y_{P1}-x_{P1}y_{P2})\times 0}\omega_i$	$\varnothing$:No solution of equation

The wear of the jaws and the size deviation of the steel arch would easily lead to insufficient grasping accuracy, derived by which, the grasping force would even fail to meet the grasping requirements of the steel arch. With the adjunction of a prismatic DOF to the upper jaw, a force sensor is also installed to guarantee the grasping effect. 4 types of grasping module structures are shown in Fig. 6.

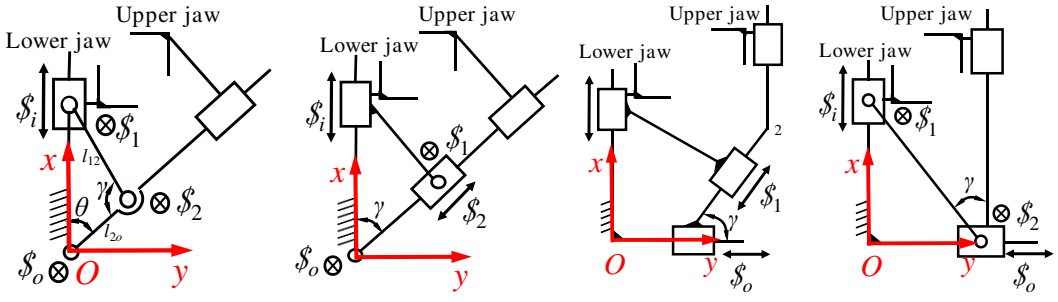

(a) PRRR_P (b) PRPR_P (c) PPP_P (d) PRRP_P

Fig. 6 Optional structure of grasping module

3.2 Design of the docking module

Following with the grasping action, the splicing manipulator is required to adjust and dock the steel arch. Driving the grasping module to complete the corresponding spatial rotation and lateral movement by the docking module, the grasping posture would be adjusted and the steel arch would also be docked. According to the action

requirement of the docking module, the freedom space could be obtained by applying the graphical type synthesis method. In addition, based on the functional equivalence of the space line diagram, the same-dimensional subspace of the docking module is derived while the corresponding kinematics pair is also obtained, as shown in Fig.7.

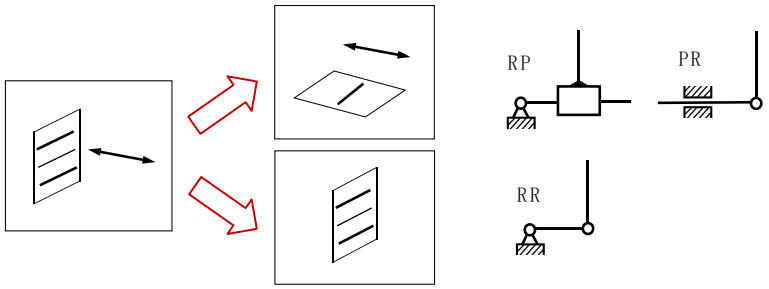

Fig.7 The kinematics pair corresponding to the freedom space of the grasping module

3.3 Optional configuration of steel arch splicing manipulator

Combining the grasping module and the docking module, 12 basic structure forms of steel arch splicing manipulators that can meet the requirements of single steel arch splicing motion are obtained, as shown in Fig.8.

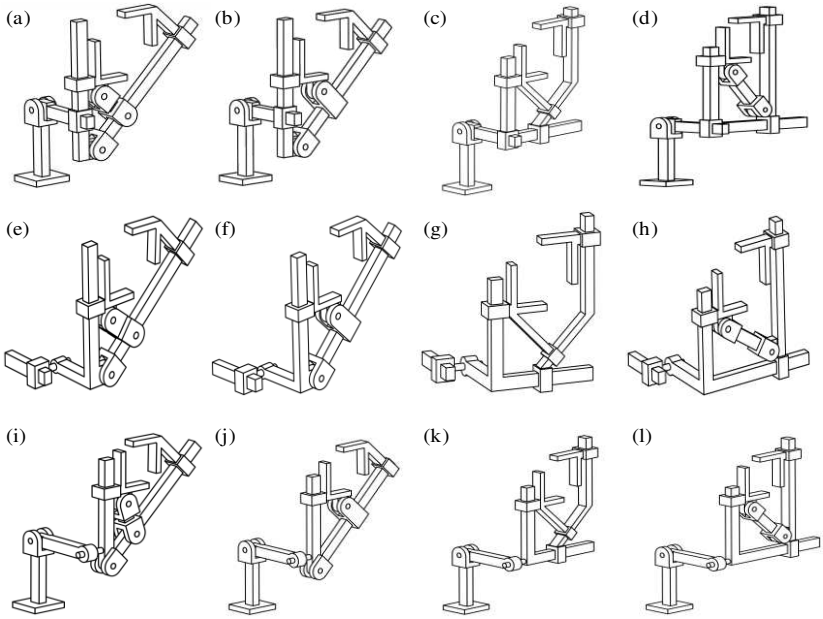

Fig.8 Single side basic structures of steel arch splicing manipulators

All the mentioned 12 steel arch splicing manipulators could realize the grasping and docking actions of the steel arch through distinct working methods, additionally, the design requirements of the steel arch splicing manipulator could also be satisfied at the meanwhile. However, due to the difference in structure, each manipulator is endowed with different performance during the manufacturing and construction. In light of this,

corresponding indices are needed to be proposed and evaluated.

4 Optimal configuration of steel arch splicing manipulator

4.1 Evaluation of motion/force transmission indices of grasping module

With a relatively complicated structure of the grasping module closed-loop mechanism, the motion/force transmission characteristics need to be analyzed to ensure the grasping requirements of the steel arch splicing manipulator could be satisfied.

(1) Local transmission index

In the closed-loop mechanism of the grasping module, the kinematic pair screws except the input screw $\$_i$ and output screw $\$_o$ are linearly independent, by which a screw system $\{\$_1, \mathrm{L}\ ,\$_n\}$ could be formed. According to the screw theory, the transmission force screw $\$_T$ could be obtained. $\$_T$ is reciprocal to $\$_1$, … ,$\$_n$, and independent with the linearity of the constraint-screw system of the closed-loop mechanism.

Define the input transmission coefficient ς and output transmission coefficient σ respectively as[37]

$$\begin{cases} \varsigma = \dfrac{|\$_i \circ \$_T|}{|\$_i \circ \$_T|_{\max}} \\ \sigma = \dfrac{|\$_o \circ \$_T|}{|\$_o \circ \$_T|_{\max}} \end{cases} \tag{25}$$

The local transmission index of the mechanism could be defined as

$$\chi = \min\{\varsigma, \sigma\} \tag{26}$$

(2) Global transmission index

The local transmission index could only judge the effectiveness of motion/force transmission of the grasping module with a single posture. However, the grasping module operates in a continuous working space. In order to judge the motion/force transmission in the entire working space, the global transmission index is defined as

$$\Gamma = \frac{\int_W \chi \mathrm{d}W}{\int_W \mathrm{d}W} \tag{27}$$

where χ is the local transmission index, and W is the working space.

The motion/force transmission analysis is carried out on the single-DOF closed-loop structures of 4 kinds of grasping modules. With the purpose of better motion/force transmission, the transmission angle γ adopts the most widely accepted range of [45°, 135°]. As shown in Fig.6(a), regarding to the grasping module PRRR_P, $\theta \in [45°, 90°]$. In order to enable the transmission angle γ to meet the requirements and ensure the transmission efficiency, it is necessary to set $l_{12} = \sqrt{2} l_{2o}$. The transmission performance of the closed-loop structures of the

grasping module is shown in Table 4, where $(x_i \quad y_i)$ is the position or movement direction of joint *i* in the coordinate system, l_{ij} is the distance between joint *i* and joint *j*, and the angles represented by θ and γ are shown in Fig. 6.

Table 4 Motion/force transmission performance of the closed -loop structure of the grasping module

Type of grasping module	Expression of $\$_{\mathbf{T}}$	Variable range	$\chi=\min\{\varsigma,\sigma\}$	Γ
PRRR_P	$\$_{\mathbf{T}}=(x_2-x_1 \quad y_2 \quad 0;\ 0 \quad 0 \quad x_1y_2)$	$\theta\in[45°,90°]$	$\min\left\{\frac{2\sqrt{3}}{3}\lvert\cos(\gamma+\theta)\rvert,\sin\gamma\right\}$	0.8803
PRPR_P	$\$_{\mathbf{T}}=\left(-\sin\gamma \quad \cos\gamma \quad 0;\ 0 \quad 0 \quad \frac{y_1}{\sin\gamma}\right)$	$\gamma\in[45°,90°]$	$\min\left\{\sin\gamma,\frac{1}{\sqrt{2}\sin\gamma}\right\}$	0.7563
PPP_P	$\$_{\mathbf{T}}=(-y_1 \quad x_1 \quad 0;\ 0 \quad 0 \quad 0)$	$x_1\in[0,l_{2o}\sin\gamma]$	$\min\left\{1,\frac{x_1}{l_{2o}\sin\gamma}\right\}$	0.5000
PRRP_P	$\$_{\mathbf{T}}=(-x_1 \quad y_2 \quad 0;\ 0 \quad 0 \quad x_1y_2)$	$\gamma\in[45°,90°]$	$\min\left\{\sqrt{2}\cos\gamma,\sin\gamma\right\}$	0.4957

Defining the high-quality motion/force transmission mechanism as a mechanism with a global transmission index Γ which is not less than 0.7. It could be seen from Table 4 that the grasping modules PRRR_P and PRPR_P are both high-quality motion/force transmission mechanisms.

4.2 Complexity evaluation of steel arch splicing manipulator

In addition to the motion/force transmission performance, it is also necessary to analyze the mechanical complexity of the steel arch splicing manipulator to gain the best solution with low topology complexity, high performance as well as the low drive system complexity. The structural complexity evaluation indices of the steel arch splicing manipulator are proposed as follows:

(1) *Joint-number complexity*, K_N

$$K_N=1-\exp(-q_N N) \tag{28}$$

where *N* is the number of joints in the steel arch splicing manipulator, and q_N is the resolution parameter defined by

$$q_N=\begin{cases}-\ln(0.1)/N_{\max}, & \text{for } N_{\max}>0;\\ 0, & \text{for } N_{\max}=0.\end{cases} \tag{29}$$

(2) *Joint-type complexity*, K_J

$$K_J=\frac{1}{n}\left(n_R K_{G|R}+n_P K_{G|P}\right) \tag{30}$$

where n_R and n_P are the numbers of revolute and prismatic joints, respectively with $n=n_R+n_P$. $K_{G|x}$ is the

geometric complexity of the pair *x* as introduced in [39]: $K_{GR}=0.5234$, $K_{G|P}=1$.

(3) *Link diversity*, K_B

Link diversity K_B is defined to quantify the geometric constraints between neighboring joints. For a revolute joint, its axis of rotation is considered whereas for a prismatic joint, its direction. Five possible joint-constraint types between the neighboring joint axes/directions are reported in[39]:

Type B_1: Orthogonal intersection.

Type B_2: Nonorthogonal intersection.

Type B_3: Parallelism.

Type B_4: Orthogonal but not intersecting.

Type B_5: Skew.

Link diversity K_B of steel arch splicing manipulator could be expressed as

$$K_B=\frac{B}{B_{\max}},\ B=-\sum_{i=1}^{c}b_i\log_2\left(b_i\right),\ b_i=\frac{M_i}{\sum_{i=1}^{c}M_i} \tag{31}$$

where B is the entropy of the joint-constraint types and $B_{\max}=2.3219$ [40]. c is the number of distinct joint-constraint types and M_i is the instance number of each type of joint-constraints.

(4) *Actuator-number complexity*, K_A

$$K_A=1-\exp\left(-q_A A\right),A=a-a_m \tag{32}$$

where a is the number of actuators in the robot topology at hand, while a_m is the minimum number of actuators allowed.

$$q_A=\begin{cases}-\ln\left(0.1\right)/A_{\max}, & \text{for } A_{\max}>0;\\ 0, & \text{for } A_{\max}=0.\end{cases} \tag{33}$$

(5) *Operation mode complexity*, K_{OM}

The operation complexity K_{OM} is specifically defined for the steel arch splicing manipulator. During the docking process of the steel arch, the designed steel arch splicing manipulators are endowed with two different operation modes. The first operation mode(OM1) is that the left and right docking modules drive a prismatic pair respectively, so as to drive the steel arch to dock along a straight line, as shown in PR and RP structure in Fig.7.The second operation mode(OM2) is to drive both revolute pairs at the same time, as shown in RR structure in Fig.7. It could be seen that the motion trajectory is difficult to control with the application of the later mode, additionally, the internal interference would also be pronely caused. In this paper, the problem would be

analyzed by introducing a new complexity index K_{OM} .

$$K_{OM}=0 \text{ for OM1} \tag{34}$$

$$K_{OM}=1 \text{ for OM2} \tag{35}$$

(6) *Total complexity*, *K*

Total complexity $K\in[0, 1]$ is defined as a convex combination of the different complexity indices. It is defined as

$$K = w_N K_N + w_J K_J + w_B K_B + w_P K_P + w_{OM} K_{OM} \tag{36}$$

where w_N , w_J , w_L , w_B , w_P and w_{OM} denote their corresponding weights, such that

$$w_N + w_J + w_B + w_P + w_{OM} = 1 \tag{37}$$

Assigning equal weights to all complexity indices implies

$$K = \frac{1}{5}\left(K_N + K_J + K_B + K_P + K_{OM}\right) \tag{38}$$

According to the evaluation results of the motion/force transmission indices of the grasping module, it could be found that the splicing manipulators *a*, *b*, *e*, *f*, *i*, *j* present an outstanding performance. The structural complexity analysis of these 6 steel arch splicing manipulators is shown in Table 5. It could be seen that due to the different Operation modes of steel arch docking, the complexity of the latter two steel arch splicing manipulators is significantly higher than the first four. Among them, the complexity of manipulator *j* reaches the highest as 0.6911. On the contrary, the complexity of the steel arch splicing manipulator *b* reaches the minimum value of 0.4228, which is mainly accounted by the smaller K_B and K_{OM} comparing to other configurations, which witness a better performance.

Table 5 Complexity indices of the manipulators

	K_N	K_J	K_B	K_A	K_{OM}	K
a	0.9	0.7274	0.8277	0	0	0.4910
b	0.9	0.7957	0.4182	0	0	0.4228
e	0.9	0.7274	0.6555	0	0	0.4566
f	0.9	0.7957	0.5904	0	0	0.4572
i	0.9	0.6596	0.6555	0	1	0.6430
j	0.9	0.7274	0.8277	0	1	0.6911

After a comprehensive comparison between both the motion/force transmission performance indices and complexity indices of the steel arch splicing manipulator, it could be obtained that the work performance of the steel arch splicing manipulator *b* is better than others. Therefore, it would be regarded as the optimal basic configuration.

4.3 Structure and working mode of steel arch splicing manipulator

The steel arch splicing manipulator is required to grasp two steel arches at the same time, hence the manipulator *b* is arranged symmetrically. Inside an extremely narrow working space of steel arch splicing, it is needed to conduct the transporting and splicing of steel arch. In order to avoid interference between the steel arch and the manipulator during transportation, the designed splicing manipulator must own the ability to stay away from the steel arch transportation track. Realized by means of joint rotation, the complete structure of steel arch splicing manipulator is shown in Fig.9.

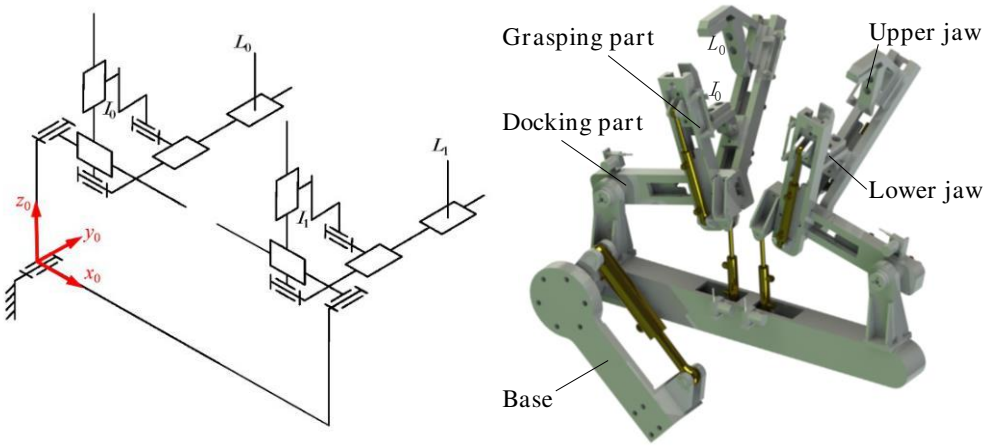

(a) Mechanism (b) Structure of steel arch splicing manipulator

Fig.9 Schematic diagram of steel arch splicing manipulator

Fig.10 displays the grasping and docking process of the steel arch splicing manipulator. While transporting the steel arch, the manipulator would rotate and get folded as shown in Fig.10(a). In terms of the grasping process, the manipulator would reach the designated position through the revolute joint, accompanying with which the grasping module opens at the meanwhile. After the steel arch enters the grasping module, the upper jaws would close as the lower jaws move upward to complete the grasping of the steel arch, as shown in Fig.10(b). Simultaneously dragging the two grasped steel arches towards the middle, the docking operation of the steel arches would be completed as shown in Fig.10(c).

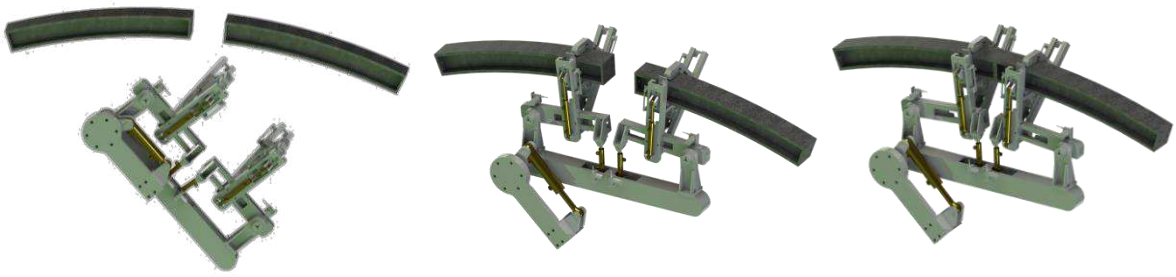

(a) Folding (b) Grasping (c) Docking

Fig.10 Working process of steel arch splicing manipulator

5 Prototype manufacturing and in-plant testing

5.1 Trial production of steel arch splicing manipulator

According to the research results, a prototype of the steel arch splicing manipulator is designed and manufactured. The prototype is applied to TBM in a TBM manufacturing plant. The position and pose of the jaws are controlled by the hydraulic cylinder. It can realize the grasping, adjusting and docking of steel arch.

The distribution of the cylinders of the steel arch splicing manipulator is shown in Fig.11. According to different functions, it could be divided into 5 types:

No. 1 cylinder is the rotating cylinder of the steel arch splicing manipulator, which is used to control the steel arch splicing manipulator to avoid the transportation track of the steel arch.

No. 2 cylinder is the posture adjustment cylinder, which is used to adjust the posture angle of the grasped steel arch.

No. 3 cylinder is the docking cylinder, which is used to push the grasping modules to enable the docking operations by the steel arches on the two grasping modules.

No. 4 cylinder is the lower jaw control cylinder, which is used to control the up and down movement of the lower jaw and simultaneously adjust the opening angle of the grasping module.

No. 5 cylinder is the upper jaw control cylinder, which is used to control the movement of the upper jaw and realize the grasping operation of the steel arch.

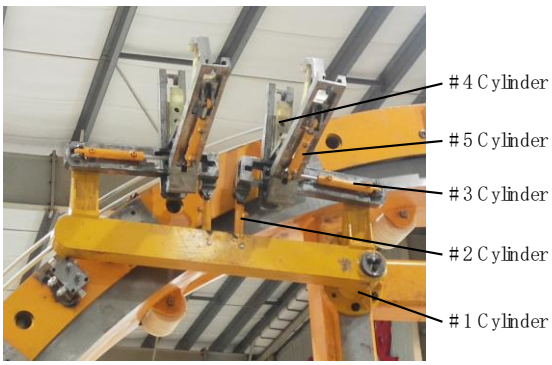

Fig.11 Steel arch splicing manipulator prototype

5.2 In-plant tests

The steel arch splicing manipulator prototype is applied to carry out the steel arch grasping and docking experiment, as shown in Fig.12. When the manipulator is in contact with the steel arch, it is necessary to reduce the cylinder speed to ensure the smooth operation. Furthermore, the motion control of each hydraulic cylinder during the experiment is shown in Table 6.

(a) TBM steel arch splicing test bench (b) Steel arch splicing test

Fig. 12 TBM steel arch splicing test

Table 6 Control parameters of each cylinder at different stages

stage	time/s	#1/(mm·s^{-1})	#2/(mm·s^{-1})	#3/(mm·s^{-1})	#4/(mm·s^{-1})	#5/(mm·s^{-1})
1	0~10	14	0	0	0	0
2	10~20	0	0	0	-12.5	12
3	20~30	0	13	0	0	0
4	30~50	0	0	0	6.25	-5
5	50~70	0	0	6.25	0	0

Specifically in this table, the positive number indicates the cylinder stretch, while the negative number implies the cylinder contraction.

The splicing test of 2 steel arches is divided into 5 stages: The No. 1 cylinders are stretched to realize the rotation of the splicing manipulator between 0-10s. While at 10-20s, the No. 4 cylinders are contracted with the stretch of No. 5 cylinders, meanwhile the jaws are expanded to prepare for the grasping of the steel arches. In the following period between 20~30s, the stretch of No. 2 cylinders enables the jaws to be lifted and gradually approach the steel arches. At 30~50s, the No. 4 cylinders are stretched and the No. 5 cylinders are contracted, while at the meanwhile, the tightened jaws would tightly hold the inside steel arches. Finally, during 50~70s, the No. 3 cylinders are stretched and pull the steel arches toward the middle to realize the docking of the steel arches.

Combined with Adams software and input the cylinder control parameters of each stage, the motion trajectory of the upper jaw L_0 and the lower jaw I_0 can be clearly obtained, as shown in Fig.13.

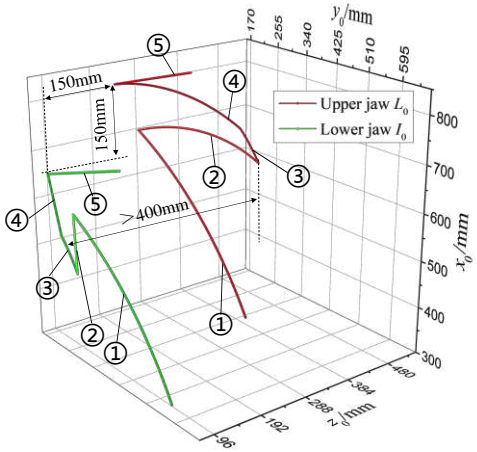

Fig.13 Motion trajectory of lower jaw I_0 and upper jaw L_0

It could be seen that the motion trajectory of the upper jaw L_0 is similar to that of the lower jaw I_0, but in stage 2 and 4, the upper jaw L_0 increases the motion along the z_0 axis, which is used to realize the separation and approach between the upper jaw and the lower jaw. During the stage 3, the distance between I_0 and L_0 exceeds 400mm, which presents as the farthest and much larger than the steel arch width of 150mm. Hence, the technical requirements could be satisfied by avoiding the collision when the steel arch splicing manipulator approaches the steel arch. Additionally at the stage 5, where the steel arch splicing manipulator has grasped the steel arch, the distance between I_0 and L_0 in both the horizontal and vertical directions reaches 150mm and meets the grasping conditions.

The experimental results show that the entire splicing process of the steel arches would occupy 70s with a relatively high efficiency. During the grasping process of the steel arches, there is no steel arch sliding and manipulator interference, which proves a grasping effect. While during the docking process, the alignment effect of the pin holes of the steel arch is excellent with the distance between the center axis of the hole less than 5mm, which meets the accuracy requirements of the steel arch.

Regarding to the practical tunnel construction, the excessive weight of the steel arch would increase the difficulty of manual handling and adjustment, in light of which even jacks and other devices would be needed as assistance. The manual connection of two adjacent steel arches would take around 5-10 minutes, compared with which the splicing efficiency of the steel arch splicing manipulator is increased by 4 to 8 times. Hence, with the application of the splicing manipulator, the construction process could be greatly accelerated.

6 Conclusions

This paper combines screw theory and graphical type synthesis method to design the steel arch splicing manipulator. Due to the large volume and mass of steel arches, in order to ensure the splicing positioning

accuracy of the manipulator and increase its structural stiffness, a single-DOF closed-loop plane mechanism is added into the grasping structure of the manipulator. Based on the basic principle of structural synthesis, a solution model of the single-DOF closed-loop mechanism is proposed. Using the screw theory, the unknown part structure of the closed-loop mechanism is deduced reversely.

The steel arch splicing manipulator is divided into two parts: grasping module and docking module. From the point of view of reducing input control, a grasping module design method with single-DOF closed-loop structure is proposed based on the derived solution model. All grasping modules that satisfy the conditions are derived in the case that only input constraints and output requirements are known. Based on the same dimensional subspace equivalence principle of graphical type synthesis method, the design method of manipulator docking module is proposed. And based on the proposed method, 12 kinds of steel arch splicing manipulator are constructed. All of these manipulators can realize the grasping and docking of steel arches and meet the design requirements of the steel arch splicing manipulator. The motion/force transmission and structural complexity of the steel arch manipulators are analyzed and discussed, and the best scheme is selected.

In order to verify the correctness of the research, a prototype of the steel arch splicing manipulator is made. Using Adams software, the output trajectory of the end of the manipulator in space is clearly obtained. The relative spatial positions of the upper and lower jaws under different working stages are analyzed, and it is proved that the manipulator satisfies the grasping requirements. The grasping effect, docking accuracy and splicing efficiency of the manipulator are studied through the steel arch splicing experiment, which proves that the manipulator meets the design requirements.

The main contribution of this paper is to propose a manipulator which can replace the manual work to realize the steel arch splicing. The manipulator is characterized by simple structure, low manufacturing cost, simple kinematics model and so on, and has a potential application prospect. A solution model of a single-DOF closed-loop mechanism is proposed for the theoretical analysis of the steel arch splicing manipulator. This method can be used for reference for other similar closed-loop manipulator and gripper design in engineering. It has important engineering significance. In the future work, we will further study the dynamic control of the steel arch splicing manipulator.

Acknowledgements

This work was supported by the National Key Research and Development Program of China (Grant No. 2017YFB1302600), the Major Science and Technology Projects of Hunan Province (Grant No. 2019GK1010).

References

[1] Huo J, Xu Z, Meng Z, Li J, Dong J, Wang L (2020) Coupled modeling and dynamic characteristics of TBM cutterhead system under uncertain factors. Mech Syst Signal Proc 140:106664. https://doi.org/10.1016/j.ymssp.2020.106664.

[2] Yu H, Li Y, Li L (2020) Evaluating some dynamic aspects of TBMs performance in uncertain complex geological structures, Tunn Undergr Space Technol 96:103216. https://doi.org/10.1016/j.tust.2019.103216.

[3] Gong H, Xie H, Yang H (2019) A Numerical Method for Extrication Characteristics of TBM Cutter-Head with the HVC. Chin J Mech Eng 32(1):102. https://doi.org/10.1186/s10033-019-0413-z.

[4] Shi Y, Xia Y, Tan Q, Zhang Y, Qiao S (2019) Distribution of contact loads in crushed zone between tunnel boring machine disc cutter and rock. J Cent South Univ 26(9):2393-2403. https://doi.org/10.1007/s11771-019-4182-8.

[5] Tao J, Lei J, Liu C, Yuan W (2019) Nonlinear Static and Dynamic Stiffness Characteristics of Support Hydraulic System of TBM. Chin J Mech Eng 32(1):101. https://doi.org/10.1186/s10033-019-0414-y.

[6] Xia Y, Guo B, Cong G, Zhang X, Zeng G (2017) Numerical simulation of rock fragmentation induced by a single TBM disc cutter close to a side free surface. Int J Rock Mech Min Sci 91:40-48. https://doi.org/10.1016/j.ijrmms.2016.11.004.

[7] Zhu Y, Sun W, Huo J, Meng Z (2019) A New System to Evaluate Comprehensive Performance of Hard-Rock Tunnel Boring Machine Cutterheads. Chin J Mech Eng 33(1):103. https://doi.org/ 10.1186/s10033-019-0410-2.

[8] Zhang R, Chen G, Zou J, Zhao L, Jiang C (2019) Study on roof collapse of deep circular cavities in jointed rock masses using adaptive finite element limit analysis. Comput Geotech 111:42-55. https://doi.org/10.1016/j.compgeo.2019.03.003.

[9] Rahaman O, Kumar J (2020) Stability analysis of twin horse-shoe shaped tunnels in rock mass. Tunn Undergr Space Technol 98:103354. https://doi.org/10.1016/j.tust.2020.103354.

[10] Mitelman A, Elmo D (2019) Analysis of tunnel-support interaction using an equivalent boundary beam. Tunn Undergr Space Technol 84:218-226. https://doi.org/10.1016/j.tust.2018.11.021.

[11] Chen Q, Wang J, Huang W, Yang Z, Xu R (2020) Analytical solution for a jointed shield tunnel lining reinforced by secondary linings. Int J Mech Sci 185:105813. https://doi.org/ 10.1016/j.ijmecsci.2020.105813.

[12] Zhong G, Hou Y, Dou W (2019) A soft pneumatic dexterous gripper with convertible grasping modes. Int J Mech Sci 153:445-456. https://doi.org/10.1016/j.ijmecsci.2019.02.028.

[13] Huang C (2019) A general method for developing different types of 3-DOF and 6-DOF isotropic manipulators. J Chin Soc Mech Eng 40(2):99-108.

[14] Ozgür E, Gogu G, Mezouar Y (2017) A study on dexterous grasps via parallel manipulation analogy. J Intell Robot Syst 87(1):3-14. https://doi.org/10.1007/s10846-017-0481-1.

[15] Lambert P, Herder J (2019) A 7-DOF redundantly actuated parallel haptic device combining 6-DOF manipulation and 1-DOF grasping. Mech Mach Theory 134:349-364. https://doi.org/10.1016/j.mechmachtheory.2019.01.002.

[16] Gao C, Huang H, Li B, Jia G (2019) Design of a truss-shaped deployable grasping mechanism using mobility bifurcation. Mech Mach Theory 139:346-358. https://doi.org/10.1016/j.mechmachtheory.2019.05.003.

[17] Liang D, Zhang W (2018) PASA-GB hand: a novel parallel and self-adaptive robot hand with gear-belt mechanisms. J Intell Robot Syst 90:3-17. https://doi.org/10.1007/s10846-017-0644-0.

[18] Kaluarachchi M, Ho J, Yahya S (2018) Design of a single motor, tendon driven redundant manipulator with reduced driving joint torques. Mech Based Des Struct Mech 46(5):591-614. https://doi.org/10.1080/15397734.2017.1374189.

[19] Babin V, Gosselin C (2018) Picking, grasping, or scooping small objects lying on flat surfaces: a design approach. Int J Robot Res 37(12):1484-1499. https://doi.org/10.1177/0278364918802346.

[20] Yang Q, Hao G, Li S, Wang H, Li H (2020) Practical Structural Design Approach of Multiconfiguration Planar Single-Loop Metamorphic Mechanism with a Single Actuator. Chin J Mech Eng 33(1):77. https://doi.org/ 10.1186/s10033-020-00498-4.

[21]Liang C, Ceccarelli M, Takeda Y (2012) Operation analysis of a Chebyshev–Pantograph leg mechanism for a single DOF biped robot. Front Mech Eng 7(4):357-370. https://doi.org/10.1007/s11465-012-0340-5.

[22] Lokhande N, Emche V (2013) Mechanical spider by using Klann mechanism. Int J Mech Eng Comput Appl 1(5):13-16.

[23] Ottaviano E, Grande S, Ceccarelli M (2010) A biped walking mechanism for a rickshaw robot. Mech Based Des Struc 38(2):227-242. https://doi.org/10.1080/15397731003645008.

[24] Wu J, Yao Y, Ruan, Liu X (2016) Design and optimization of a dual quadruped vehicle based on whole close-chain mechanism. Proc Inst Mech Eng Part C-J Eng Mech Eng Sci 231(19):3601-3613. https://doi.org/10.1177/0954406216650473.

[25] Wu J, Yao Y (2017) Design and analysis of a novel multi-legged horse-riding simulation vehicle for equine-assisted therapy. Proc Inst Mech Eng Part C-J Eng Mech Eng Sci 232(16):2912-2925. https://doi.org/10.1177/0954406217728300.

[26] Wu J, Yao Y (2018) Design and analysis of a novel walking vehicle based on leg mechanism with variable topologies. Mech Mach Theory 128:663-681. https://doi.:10.1016/j.mechmachtheory.2018.07.008.

[27]Liu Y, Ben-Tzvi P (2020) An articulated closed kinematic chain planar robotic leg for high-speed locomotion. J Mech Robot 12(4):041003. https://doi.org/10.1115/1.4045689.

[28] Hassan A, Abomoharam M (2014) Design of a single DOF gripper based on four-bar and slider-crank mechanism for educational purposes. Procedia CIRP 21:379-384. https://doi.org/10.1016/j.procir.2014.02.062.
[29] Hassan A, Abomoharam M (2017) Modeling and design optimization of a robot gripper mechanism. Robot Comput Integr Manuf 46:94-103. https://doi.org/10. 1016/j.rcim.2016.12.012.
[30] Anwar M, Khawli T, Hussain I, Gan D, Renda F (2019) Modeling and prototyping of a soft closed-chain modular gripper. Industrial Robot 46(1):135-145. https://doi.org/10.1108/ir-09-2018-0180.
[31] Yu H, Zhang J, Wang H (2018) Dynamic performance of over-constrained planar mechanisms with multiple revolute clearance joints. Proc Inst Mech Eng Part C-J Eng Mech Eng Sci 232(19):3524-3537. https://doi.org/10.1177/0954406217738032.
[32] Li Y, Zhang Y, Zhang L (2020) A New Method for Type Synthesis of 2R1T and 2T1R 3-DOF Redundant Actuated Parallel Mechanisms with Closed Loop Units. Chin J Mech Eng 33(1):78. https://doi.org/ 10.1186/s10033-020-00487-7.
[33] Zhou C, Fang Y (2018) Design and Analysis for a Three-Rotational-DOF Flight Simulator of Fighter-Aircraft. Chin J Mech Eng 31(1):55. https://doi.org/10.1186/s10033-018-0256-z.
[34] Yang S, Sun T, Huang T (2017) Type synthesis of parallel mechanisms having 3T1R motion with variable rotational axis. Mech Mach Theory 109:220-230. https://doi.org/10.1016/j.mechmachtheory.2016.11.005.
[35] Sun T, Yang S, Huang T, Dai J (2018) A finite and instantaneous screw based approach for topology design and kinematic analysis of 5-axis parallel kinematic machines. Chin J Mech Eng 31(2):44. https://doi.org/10.1186/s10033-018-0241-6.
[36] Xie F, Liu X (2015) Design and development of a high-speed and high-rotation robot with four identical arms and a single platform. J Mech Robot 7(4):041015. https://doi.org/10.1115/1.4029440.
[37] Xie F, Liu X, Wang C (2015) Design of a novel 3-DoF parallel kinematic mechanism: type synthesis and kinematic optimization. Robotica 33(3):622-637. https://doi.org/10.1017/s0263574714000551.
[38] Zhang K, Dai J (2016) Geometric constraints and motion branch variations for reconfiguration of single-loop linkages with mobility one. Mech Mach Theory 106:16-29. https://doi.org/10.1016/j.mechmachtheory.2016.08.006.
[39] Nayak A, Caro S, Wenger P (2018) Comparison of 3-[PP]S Parallel Manipulators based on their Singularity Free Orientation Workspace, Parasitic Motions and Complexity. Mech Mach Theory 129:293-315. https://doi.org/10.1016/j.mechmachtheory. 2018.08.001.
[40] Caro S, Khan W, Pasini D, Angeles J (2010) The rule-based conceptual design of the architecture of serial schnflies-motion generators. Mech Mach Theory 45(2):251-260. https://doi.org/10.1016/j.mechmachtheory.2009.09.002.

Figures

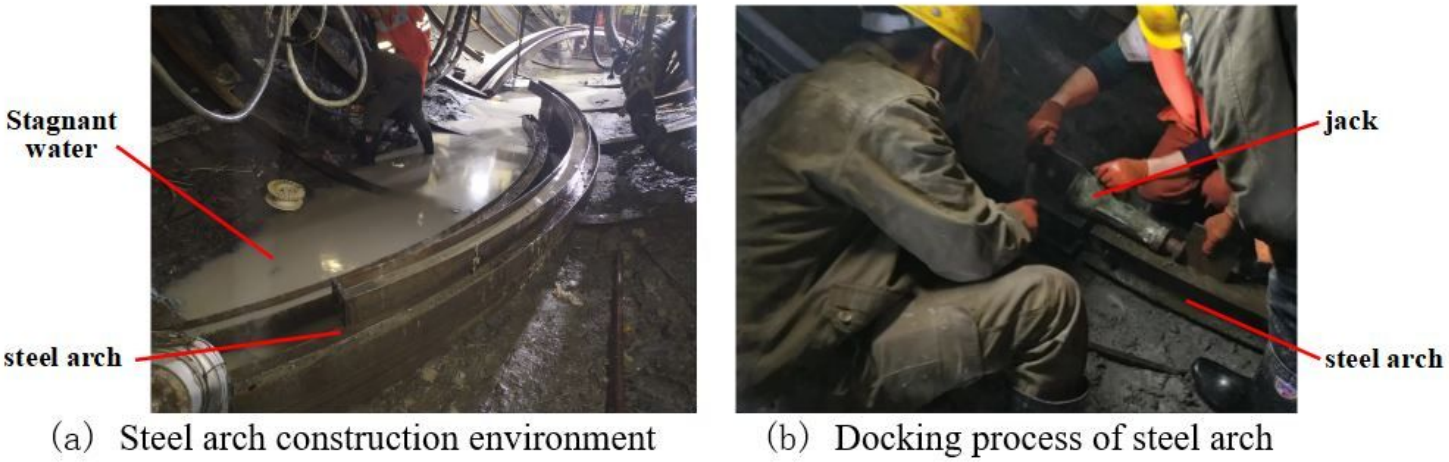

Figure 1

Manual splicing of steel arch

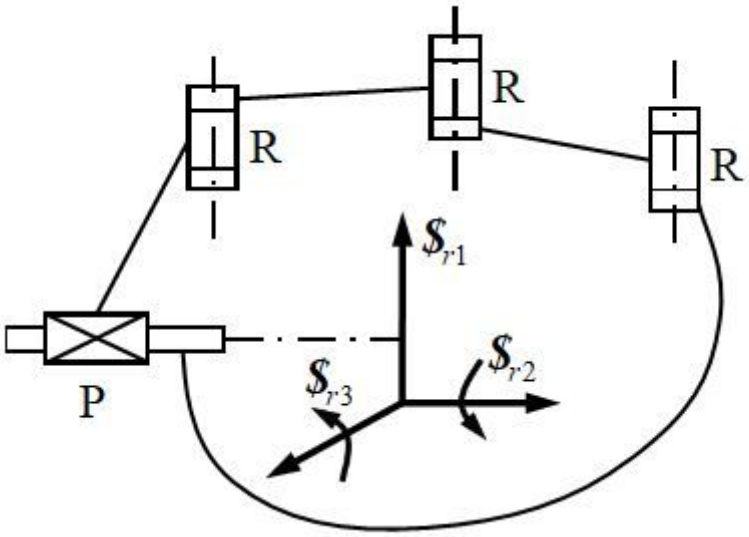

Figure 2

RRRP single-DOF closed-loop planar mechanism

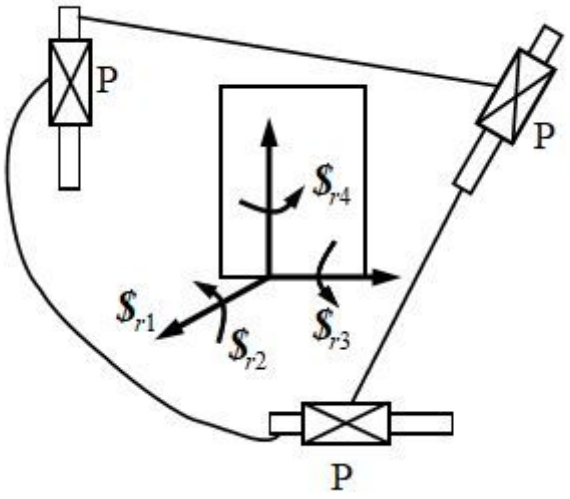

Figure 3

RRRP single-DOF closed-loop planar mechanism

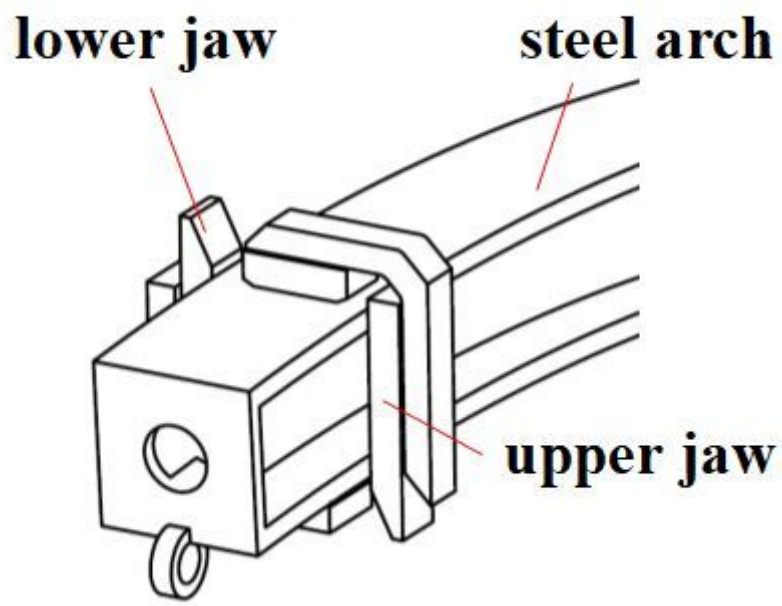

Figure 4

Schematic diagram of steel arch splicing

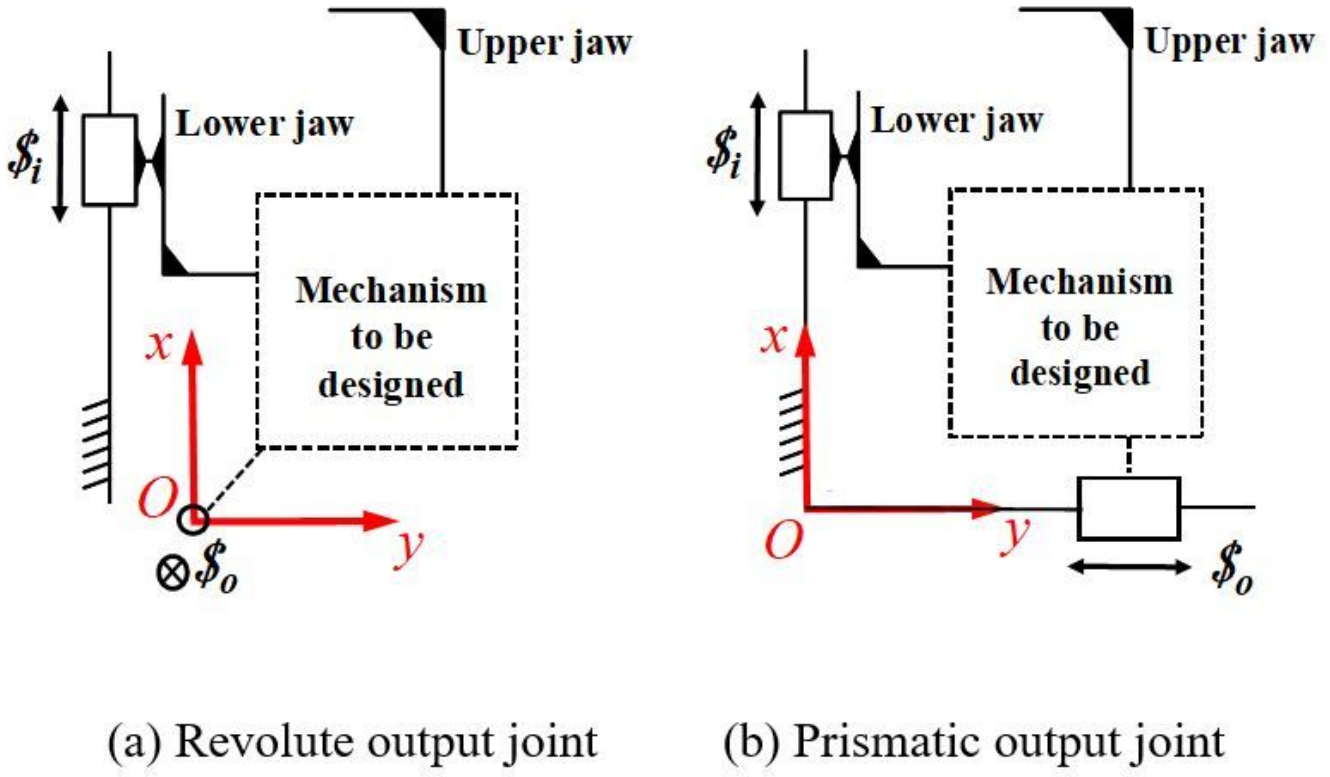

Figure 5

Schematic diagram of grasping module

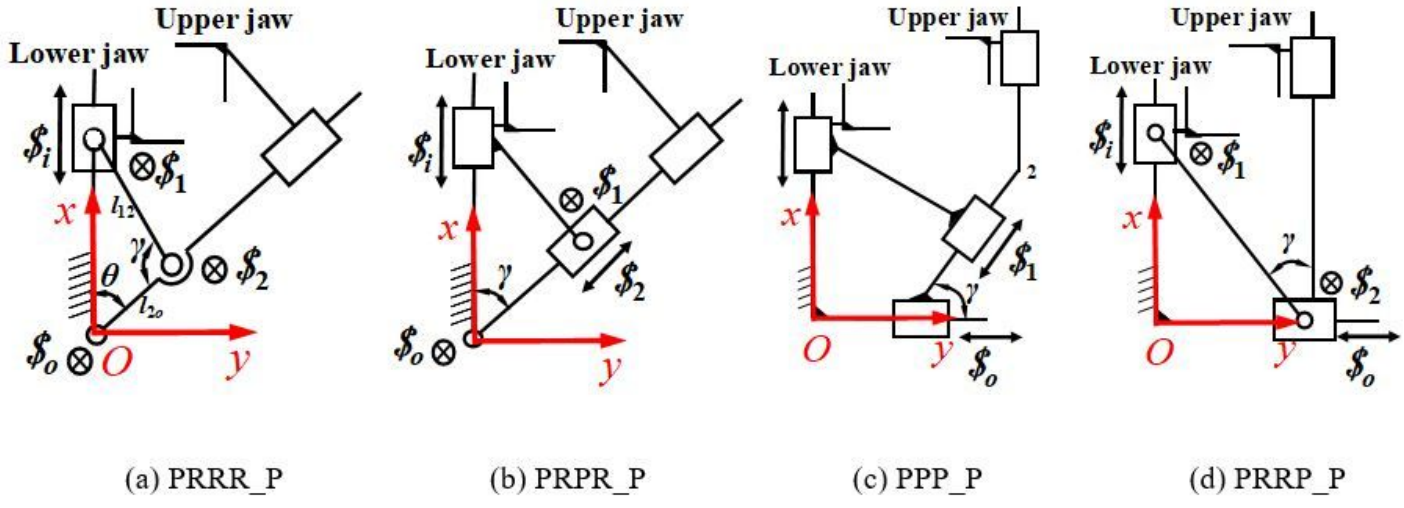

Figure 6

Optional structure of grasping module

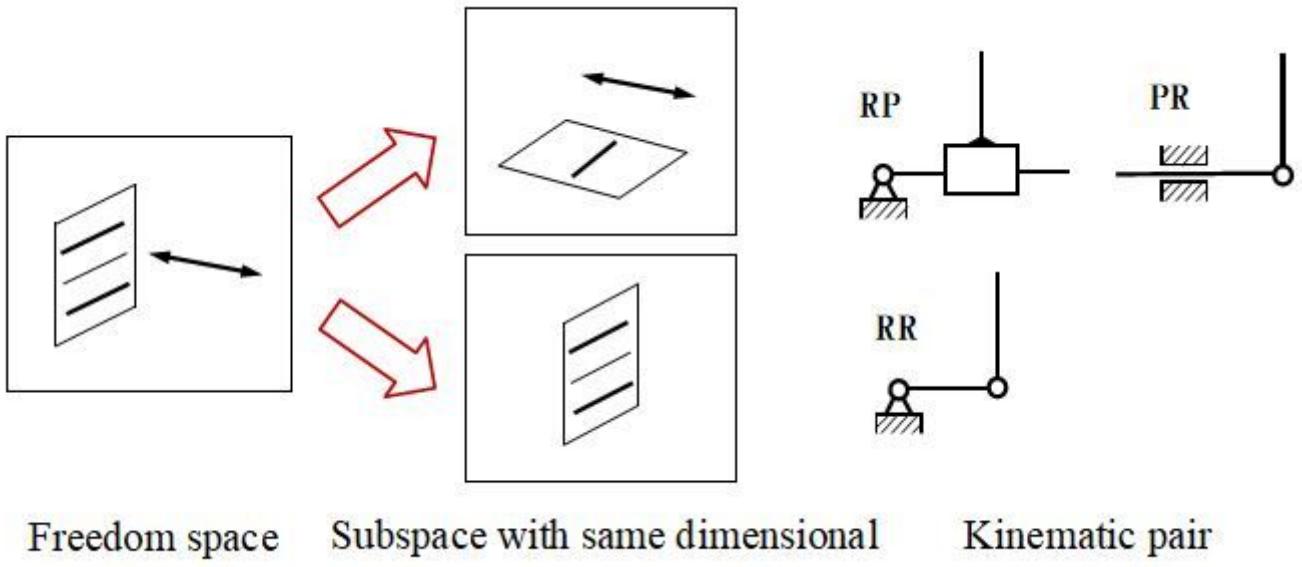

Figure 7

The kinematics pair corresponding to the freedom space of the grasping module

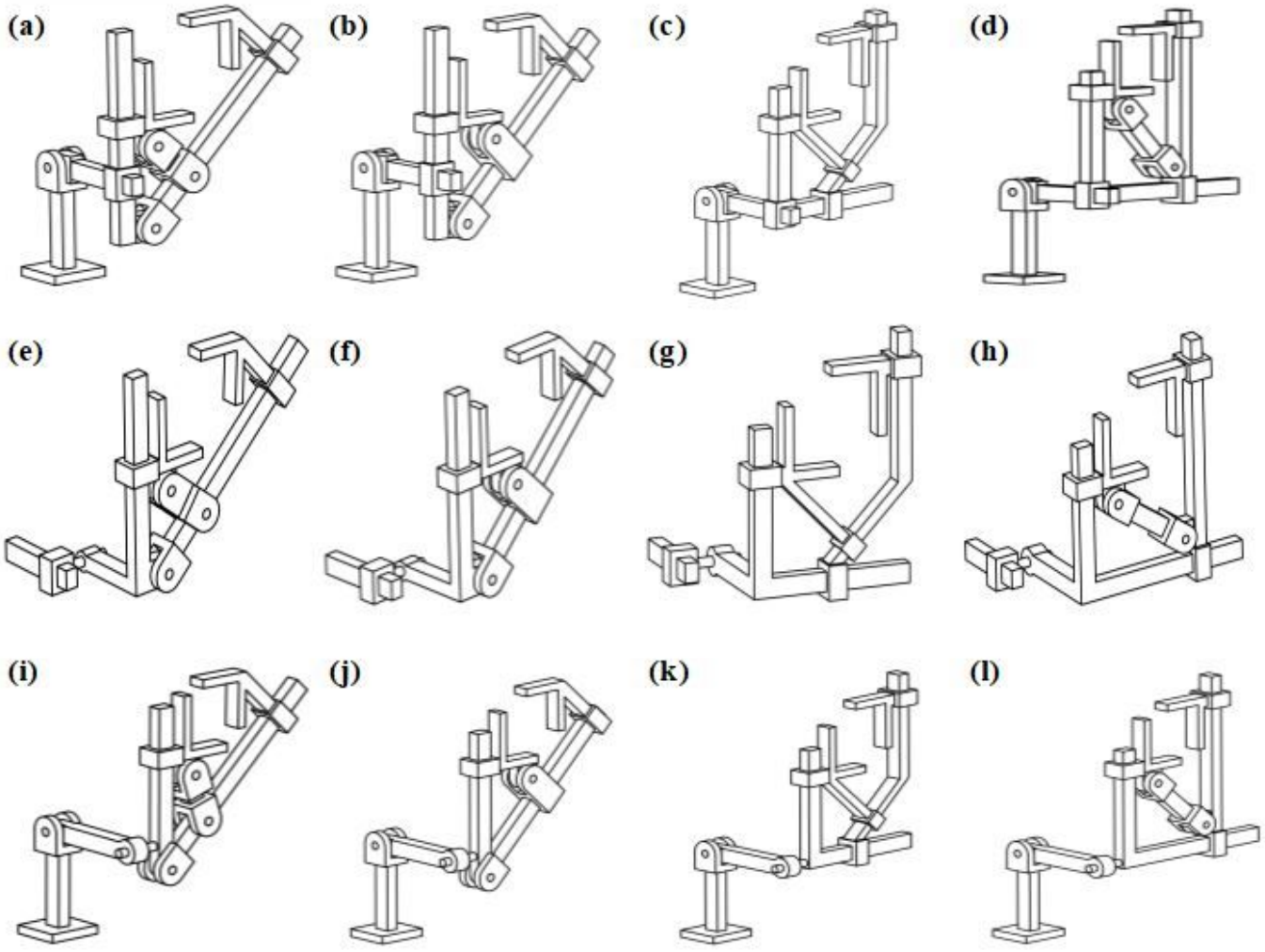

Figure 8

Single side basic structures of steel arch splicing manipulators

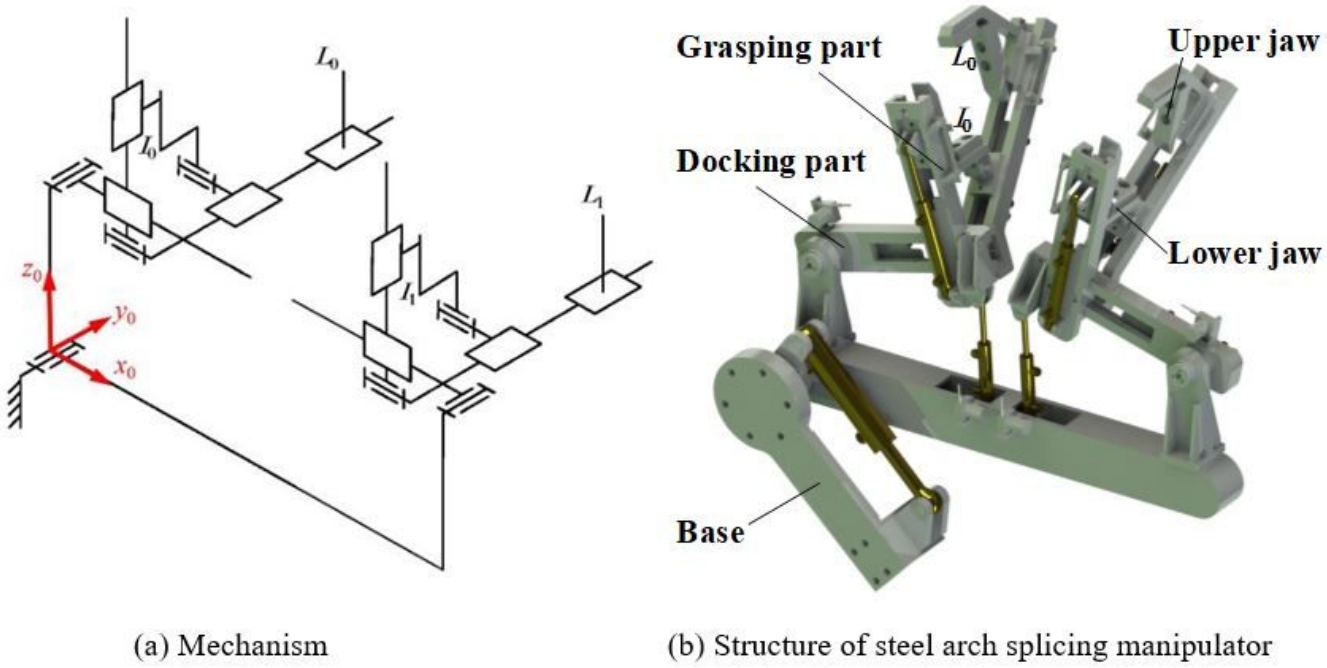

(a) Mechanism (b) Structure of steel arch splicing manipulator

Figure 9

Schematic diagram of steel arch splicing manipulator

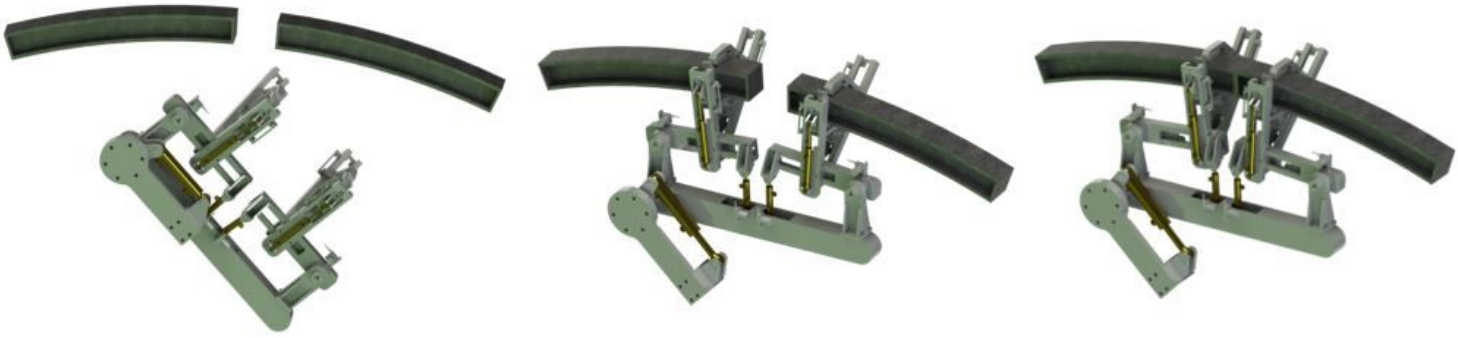

(a) Folding (b) Grasping (c) Docking

Figure 10

Working process of steel arch splicing manipulator

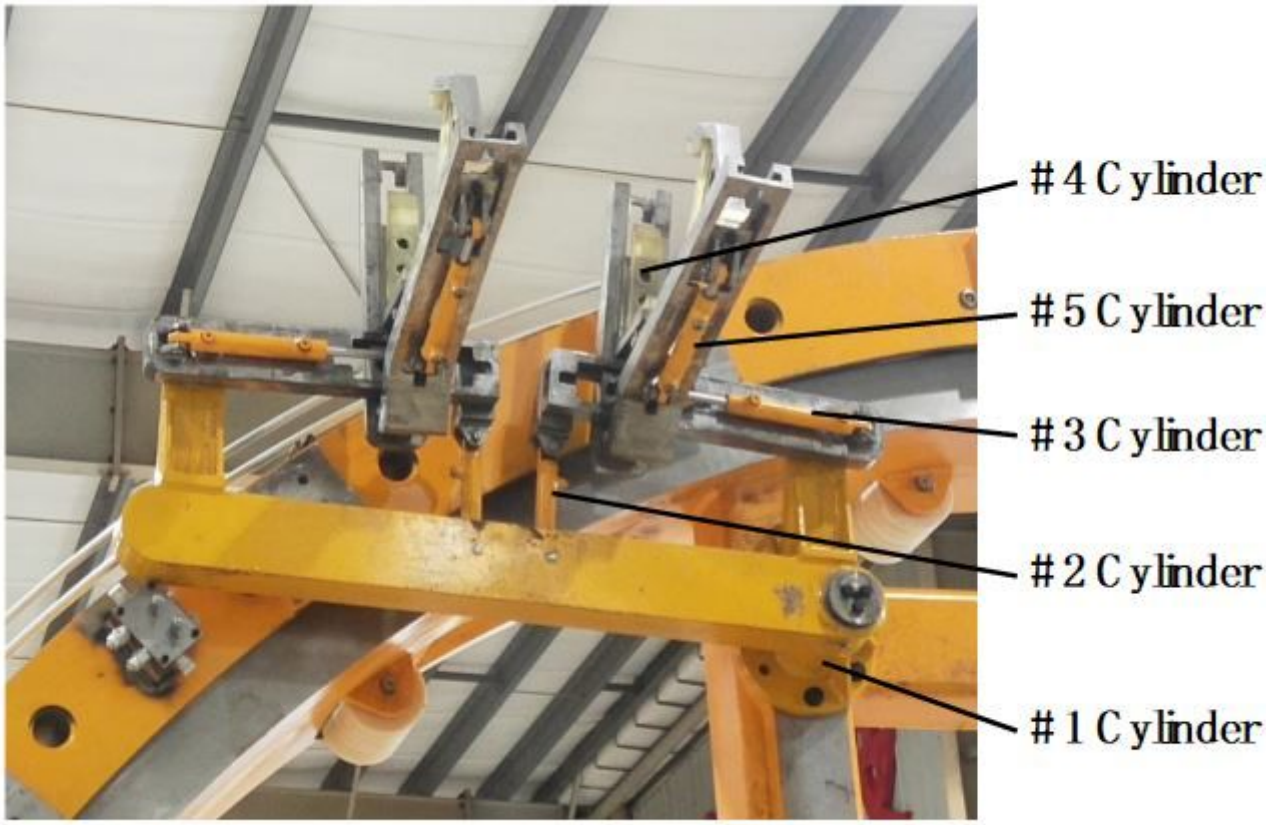

Figure 11

Steel arch splicing manipulator prototype

(a) TBM steel arch splicing test bench (b) Steel arch splicing test

Figure 12

TBM steel arch splicing test

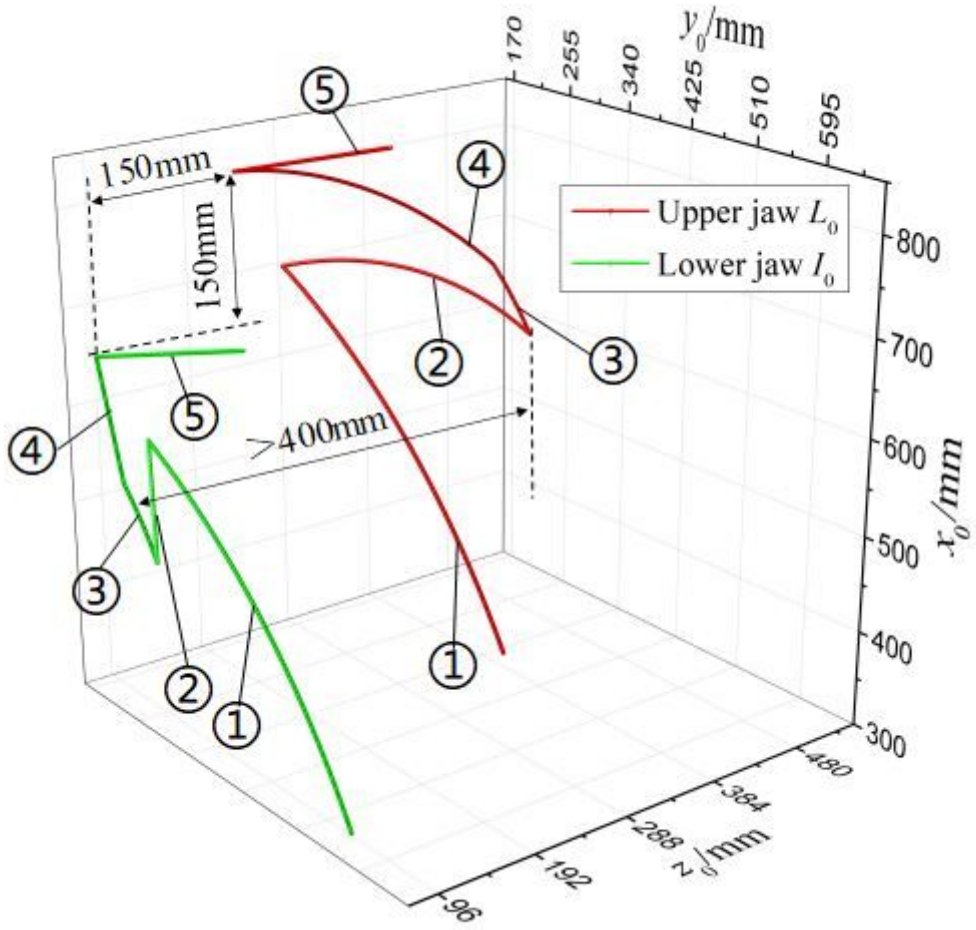

Figure 13

Motion trajectory of lower jaw l0 and upper jaw L0